An Update on Novel Quantitative Techniques in the Context of Evolving Whole-Body PET Imaging

Sina Houshmand, MD[a], Ali Salavati, MD, MPH[a], Søren Hess, MD[b], Thomas J. Werner, MSE[a], Abass Alavi, MD[a], Habib Zaidi, PhD[c,d,e,*]

KEYWORDS

• Quantification • Segmentation • Kinetic modeling • Glucose metabolism

KEY POINTS

- Quantitative PET imaging has become an integral part of the management of patients in clinical oncology over the past 2 decades.
- Accurate PET quantification is a major breakthrough and opens many avenues for clinical diagnosis, assessment of response to treatment, and therapy planning.
- In clinical oncology, quantitative PET has become a standard practice in most academic institutions, and is widely adopted in clinical trials.
- Several PET metrics have been proposed in the literature. The selection of the best metric for a specific application is still a matter of debate.
- Quantitative PET imaging will help in charting personalized treatment plans for patients and also in exploring new therapeutic opportunities in the future.

INTRODUCTION

The progress made in PET imaging during the last few decades has tremendously expanded the applications of this imaging modality in various domains in clinical and research settings. Some of these advances include the innovations in hybrid imaging modalities that combine computed tomography (CT) or MR imaging with PET to facilitate anatomic mapping of metabolic abnormalities and improve the quantitative accuracy of PET images.

The techniques used for assessment of PET images fall under 3 major categories, namely qualitative interpretation, semiquantitative measures, and absolute quantitative analysis. Qualitative interpretation is the most subjective technique because it is performed by human readers having sufficient training and expertise. Semiquantitative measures, including standardized uptake value (SUV), lesion to background ratio (target to background ratio), and other variants, are widely used in the clinic for partial quantification of PET data. The third category

Financial Statement: This work was supported by the Swiss National Science Foundation under grant SNFS 31003A-149957.

[a] Department of Radiology, Hospital of the University of Pennsylvania, 3400 Spruce Street, Philadelphia, PA 19104, USA; [b] Department of Nuclear Medicine, Odense University Hospital, Søndre Boulevard 29, Odense 5000, Denmark; [c] Division of Nuclear Medicine and Molecular Imaging, Geneva University Hospital, CH-1211, Geneva, Switzerland; [d] Geneva Neuroscience Center, Geneva University, CH-1211 Geneva, Switzerland; [e] Department of Nuclear Medicine and Molecular Imaging, University Medical Center Groningen, University of Groningen, 9700 RB Groningen, The Netherlands

* Corresponding author. Division of Nuclear Medicine and Molecular Imaging, Geneva University Hospital, Geneva CH-1211, Switzerland.

E-mail address: habib.zaidi@hcuge.ch

PET Clin 10 (2015) 45–58

http://dx.doi.org/10.1016/j.cpet.2014.09.004

1556-8598/15/$ – see front matter

utilizes various mathematical models such as nonlinear regression and Patlak-Gjedde graphical analysis for absolute quantification of PET data. The first 2 methods are prone to interreader and intrareader variability, but are practical for clinical and research use because of their simplicity.

Qualitative visual analysis is still the main methodology used for the assessment of PET images in the clinic. Visual assessment is based on the contrast between areas with tracer-avid regions and areas with lower uptake, and is mostly used in the interpretation of clinical ^{18}F-fluorodeoxyglucose (FDG)-PET studies to detect lesions with high glycolytic activity for the assessment of metabolic contrast reflecting concentration of FDG-6-phosphate in the cells. Qualitative visual assessment is simple but suffers from many shortcomings, including the need to define a threshold for disease assessment and poor intrareader and interreader agreement.[1] However, the unique features of PET technology provide the capability to perform quantitative measures in vivo. Substantial research efforts have focused on the development of appropriate methodologies to standardize PET quantification techniques to enable direct comparison from one system to another and from one place to the other.[2] Nevertheless, there are still some concerns regarding the widespread use of suboptimal quantification methods.[3] Proper quantification of PET data is essential for accurate evaluation of the extent of disease and response to treatment.[1]

The deployment of advanced quantitative PET imaging in the clinic is expected to grow as specific targeted molecular imaging probes are designed and adopted as validated approaches in various clinical applications. Since 1990, more than 310,575 PubMed entries have appeared in the literature (about half of them published during the last 7 years alone) when searching for "PET" OR "positron emission tomography" AND "quantification" OR "quantitation" OR "quantitative" (**Fig. 1**).[4]

This review highlights, from a clinical perspective, the different efforts carried out for quantification of FDG-PET data and the methods developed for optimization of these parameters.

STATIC VERSUS DYNAMIC WHOLE-BODY PET IMAGING

Static whole-body PET imaging is widely used in diagnostic procedures adopted in the clinic. Conventional acquisition protocols on current PET/CT systems include the injection of 8 to 20 mCi (296–740 MBq) of FDG and emission scanning for 2 to 4 minutes per bed position, 45 to 60 minutes postinjection following either low-dose or contrast-enhanced diagnostic quality CT scanning for attenuation correction of the PET emission scans.[5,6] Some protocols use both a low-dose CT for attenuation correction (before PET scanning) and contrast-enhanced CT (after PET scanning) to avoid the potential appearance of artifacts when using contrast-enhanced CT for

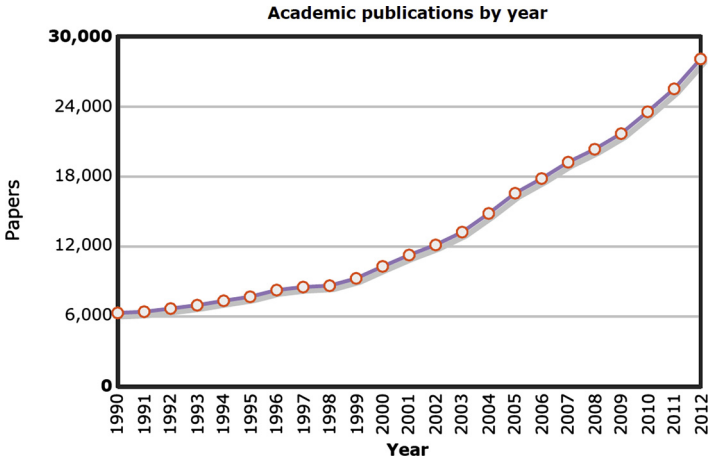

Fig. 1. The increasing number of annual peer-reviewed publications (between 1990 and 2012) reporting on developments or use of PET quantification demonstrates the growing interest in this area. This graph is based on a PubMed query with using the following MeSH terms: "PET" OR "positron emission tomography" AND "quantification" OR "quantitation" OR "quantitative". A time line was created with MEDSUM: an online MEDLINE summary tool by Galsworthy, MJ. Hosted by the Institute of Biomedical Informatics (IBMI), Faculty of Medicine, University of Ljubljana, Slovenia (www.medsum.info). (*From* Zaidi H, Alavi A. Trends in PET quantification: opportunities and challenges. Clin Transl Imaging 2014;2:184; with permission.)

attenuation correction of the PET data. Iterative reconstruction algorithms are nowadays the de facto gold-standard techniques implemented on commercial platforms.[7] The standard range of coverage for whole-body PET scanning includes the base of the skull to the mid-thigh, which requires 5 to 6 bed positions. The estimated time depends on the scanner's performance and is typically in the range of 15 to 40 minutes. Because of its simplicity, the SUV is the conventional metric used for the analysis of static whole-body clinical FDG studies. However, the SUV is unable to differentiate metabolized and nonmetabolized concentrations of tracer, and plasma dynamics is not considered in its formula.[8–10] Therefore it is only used as a semiquantitative parameter, considering its limitations in patients undergoing chemotherapy, hormone therapy, impaired renal function, and other conditions.

To address the limitations of semiquantitative analysis, various strategies for dynamic and parametric whole-body PET imaging have been explored.[11] In dynamic whole-body PET imaging, time series of PET measurements are dynamically acquired, thus enabling the estimation of physiologic parameters of interest through tracer kinetic modeling. Two approaches can be used to derive tracer kinetics from dynamic PET data: region of interest (ROI)-based kinetic modeling, which fits a model to estimated time-activity curves (TACs) of defined ROIs; and voxel-based kinetic modeling (or parametric imaging), which, by contrast, estimates kinetic parameters for each voxel, thus providing the spatial distribution of the kinetic parameters. It should be noted that parametric imaging requires substantial computational resources and is more sensitive to noise compared with ROI-based tracer kinetic modeling.[11–13]

Compared with static imaging, dynamic imaging gives considerably more information after application of image reconstruction and tracer kinetic modeling techniques. Alternatively, direct estimation of these parameters using 4-dimensional (4D) and higher-dimensional image reconstruction techniques have also been developed.[14] A novel whole-body dynamic acquisition scheme was recently introduced.[15] **Fig. 2** shows the principle of the proposed protocol, which consists of a 6-minute initial scan over the heart to extract the input function through image-based derivation of the input function (usually performed to circumvent problems associated with collecting blood samples).[16] This action is followed by dynamic whole-body scanning (6 passes) including subsequent passes over the heart. Standard Patlak linear graphical analysis modeling is then applied at the voxel level to derive parametric images reflecting tracer uptake rate (K_i). Despite much worthwhile research efforts, complexities associated with protocol design and parameter estimation has restricted the applications of whole-body dynamic PET imaging in daily practice in the clinic.[11]

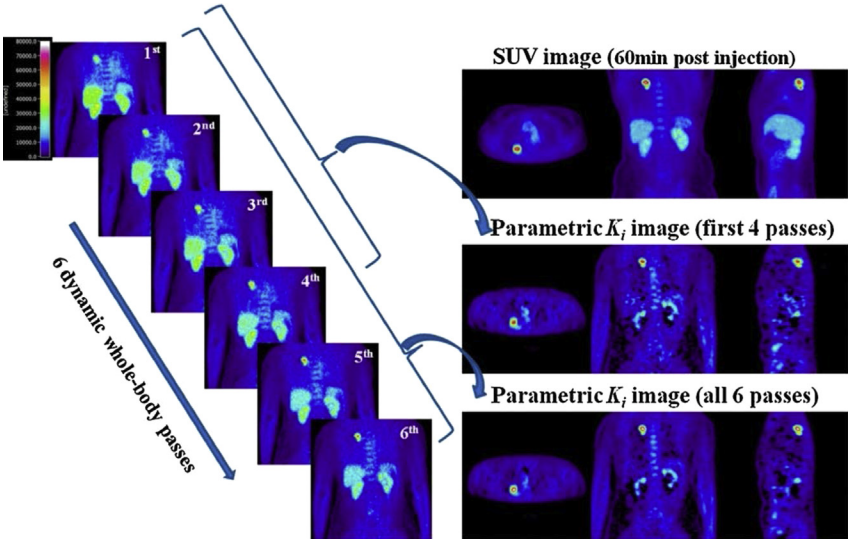

Fig. 2. (*Left*) Following a 6-minute scan of the heart (not shown), 6 whole-body passes were acquired as shown. Each pass consisted of 7 bed positions (45 seconds per bed acquisition). (*Right*) The standardized uptake value (SUV) image, the K_i parametric image derived from all 6 last frames, and the K_i image after omitting the last 2 frames are shown. (*From* Karakatsanis NA, Lodge MA, Tahari AK, et al. Dynamic whole-body PET parametric imaging: I. Concept, acquisition protocol optimization and clinical application. Phys Med Biol 2013;58:7391–418; with permission.)

TRACER KINETIC MODELING VERSUS SIMPLIFIED ANALYSIS

Quantification of Absolute Glucose Metabolic Rate

Tracer kinetic analysis determines the absolute concentration of different substrates and products in glucose metabolism and, therefore, yields the absolute rate of glucose metabolism in the cells. The advantages of kinetic modeling include the requirement to collect dynamic data, thus enabling to capture early dynamics, making the procedure less dependent on imaging time (delay after injection). However, the technique is time consuming and cumbersome to the patient because it requires a dynamic scanning protocol and arterial blood sampling.

Compartmental modeling establishes the link between the functional image and physiologic parameters of glucose metabolism. In this model, the behavior of FDG is mathematically modeled using a certain number of compartments representing various stages of FDG metabolism.[17–21] The dynamic trend of change in FDG concentration follows a 3-compartment tracer kinetic model consisting of the process of transportation and phosphorylation of FDG (**Fig. 3**). The first compartment, C_1, is considered to be an open interface having the ability to exchange FDG with various tissues in the body. Owing to the complex dynamics, it is not easy to estimate the input function, which is usually measured by arterial sampling. The second compartment, C_2, reflects the amount of FDG in the tissues ready for phosphorylation through hexokinase enzyme. After phosphorylation, FDG-6-phosphate determines the third compartment (C_3). A kinetic model is termed reversible when it accounts for dephosphorylation of FDG-6-phosphate by glucose-6-phosphatase in addition to transportation and phosphorylation. However, simplified irreversible models, which eliminate the dephosphorylation of FDG, such as nonlinear regression analysis in which a single rate constant (K_i) replaces k_1, k_2, and k_3 to estimate the net rate of FDG influx, are usually used.[22] This method, although technically complex and time consuming, is independent of imaging time after injection and enables the estimation of constants of glucose metabolism.

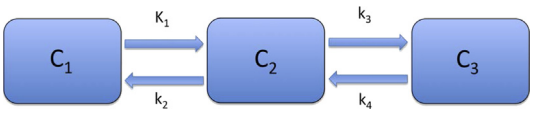

Fig. 3. Three-compartment kinetic model of ^{18}F-fluorodeoxyglucose (FDG) behavior. C_1 reflects the concentration of unmetabolized FDG in arterial plasma. The concentration of free FDG in tissue is shown by C_2, and C_3 is the concentration of FDG after phosphorylation. K_1, k_2 are the rate constants for the transportation of FDG between C_1 and C_2. K_3 is the rate with which FDG phosphorylates and k_4 the rate of dephosphorylation of FDG (usually negligible).

Patlak-Gjedde graphical analysis depicts the metabolic rate by using activity concentration, distribution volume, and net rate of influx of FDG as inputs according to the following equation:

$$c(t) = \lambda . c_p(t) + K_i \int_0^t c_p(\tau)\, d\tau$$

where $c(t)$ is activity in the tissue as measured by the PET scanner at time t, $c_p(t)$ is concentration of FDG in the plasma, λ is distribution volume of FDG, K_i is net rate of FDG influx into the tissue, and $d\tau$ is a dummy integration variable.

This method is more robust and less susceptible to noise, and is able to produce parametric images.[23] This model, however, is unable to provide details about glucose metabolism, unlike previous models.

Other more simplified kinetic models were also developed but are deemed to provide less accurate results. Sokoloff and colleagues[21] developed an autoradiographic method requiring only one static scan and arterial blood sampling.[24] Other investigators quantified glucose metabolic rates with limited blood samples.[25]

Simplified PET Quantification of Uptake Through Standardized Uptake Value

As discussed earlier, the metabolism of glucose is accurately quantified using tracer kinetic models. However, owing to the aforementioned limitations (need for dynamic data acquisition, continuous arterial blood sampling) and incapacity of conventional dynamic PET protocols to investigate more than 1 bed position at a time, dynamic whole-body PET imaging proved to be challenging. Therefore, simpler semiquantitative methods, which are easier to implement, have been developed and adopted in the clinic.

The SUV concept has been developed as a semiquantitative measure reflecting the amount of FDG uptake in a determined region after a certain time following FDG injection, normalized to the injected dose and whole-body distribution, which is mostly represented by the weight of the patient. These calculations are simple, do not need dynamic imaging and blood sampling, and are usually provided on commercial and noncommercial platforms.[26] Validation studies have also shown a linear correlation between SUV and kinetic modeling.[27,28]

Maximum SUV (SUV_{max}) is the single highest voxel/pixel in a defined region/volume of interest, whereas mean SUV (SUV_{mean}) is the average amount of SUV in all voxels/pixels in an ROI or volume of interest. The factors influencing SUV measurements include extravasation of the radiotracer at the injection site, residual activity in the syringe, difference between the clock of the dose calibrator and the PET acquisition console, and decay from the time of activity measurement to injection (if not appropriately taken into account). These factors may lead to measurement errors.[29,30]

SUV is usually normalized to body weight. However, because adipose tissue has minimal metabolic activity and accumulates FDG minimally in comparison with other active regions, it might be a source of inaccuracy in obese patients. As such, in obese patients with a higher proportion of body fat, SUV may overestimate metabolic activity in nonadipose tissue. Some studies have shown superior results with SUV normalized to body surface area or lean body mass.[9,31,32]

Elevated blood glucose level is another factor influencing SUV. Administering insulin in advance of injecting FDG in patients with type 2 diabetes increases glycolysis in muscle and adipose tissue and reduces the SUV in other tissues, owing to lower available levels of FDG. Current protocols used in most PET facilities exclude patients with blood glucose levels higher than 150 to 200 mg/dL (~8–11 mmol/L).[33]

Because the tracer may be diversely distributed within the ROI, as is the case in heterogeneous tumors, SUV_{max} tends to overestimate the mean metabolic activity of a lesion and is more sensitive to noise. However, measuring SUV_{mean} is much more operator dependent and more sensitive to partial volume effect. Therefore, automated PET image segmentation algorithms enabling definition of the contours of lesions have become highly desirable in recent years.

Effect of Physical and Physiologic Factors on Standardized Uptake Value Calculations

SUV is the most widely used PET metric in the clinic. However, this measure is affected by many physiologic and physical factors, which cause variations in the outcome of clinical trials incorporating these measures in their protocols.[30]

The physiologic factors include: the effect of blood glucose level, resulting in underestimation of the SUV with increasing blood glucose level; increased uptake period between injection and start of the PET study, which increases the SUV; and patient motion and breathing that result in mismatches in the PET and corresponding CT images used for attenuation correction. Lower SUV and resolution loss occur with respiratory motion. Patient stress and uncomfortable waiting conditions cause increased uptake in muscle and brown fat, affecting SUV measurements. Inflammatory processes close to the tumor might also cause false-positive results.[30]

The physical factors affecting the accuracy of SUV include variations in the scan acquisition parameters influencing the spatial resolution and signal-to-noise ratio (SNR). Decreased SNR causes upward bias of SUV. Changes in image reconstruction parameters affecting convergence rate and spatial resolution also affect the SUV, and might result in increased partial volume effects by making the SUV more dependent on surrounding activity distributions. The size and shape of the ROI used also affects the outcome of SUV. The normalization factors used for the calculation of SUV such as body weight, body surface area, and lean body mass directly affect the SUV. In addition, application of contrast agents and the presence of metallic artifacts in CT images overestimate the attenuation factors and cause upward bias of the SUV.[30,34–36]

Effect of Respiratory Motion on Standardized Uptake Value

Respiratory motion is another factor affecting the accuracy of PET/CT imaging, which is more prominent in cases with lesions located in the thorax or upper abdomen, affecting their diagnosis and staging. The misalignment between PET and CT images caused by respiratory motion has proved to be a challenging issue in the clinical setting.[37,38]

Current-generation CT scanners are able to scan more than 100 cm in the craniocaudal axis in 20 seconds with high-speed gantry rotation and broad detector coverage. On the other hand, PET requires 2 to 5 minutes for each bed position (16 cm to scan). The difference in temporal resolution of the CT (1 second) and PET (1 respiratory cycle) also contributes to misregistration of lesions, leading to compromised quantification.[26]

Respiratory gating can remedy the issue of misregistration by reducing motion artifacts. In 4D PET/CT, both PET and CT images are recorded through synchronization with respiratory motion in a gated mode (similarly to the schemes used in cardiac gating), and data corresponding to each breathing cycle are distributed in time bins (8–10 time bins). Each bin corresponds to 1 phase of the breathing cycle.[39]

However, the application of 4D PET has been limited because of the relatively long total acquisition time. Additionally, it is difficult for the patients

to keep the posture of holding their arms over their head for long time, which might compromise PET data acquisition. By splitting the 4D PET data into separate bins, fewer coincidence events will be acquired for each bin, causing a lower SNR.[39] All of these factors along with the prolonged post-processing time have limited the widespread clinical use of 4D PET/CT.

Effect of Partial Volume Effect and Its Correction

Partial volume effect (PVE) results from the limited spatial resolution of the PET scanner, causing lesions to differ from their real appearance and reducing their metabolic activity. Firstly, the 3-dimensional blurring produced by the PET scanner's spatial resolution makes smaller lesions appear larger in size but dimmer in signal intensity, owing to a spillover effect from the actual source to the surroundings (**Fig. 4**). This blurring effect is even more pronounced for moving lesions because of respiratory or cardiac motion. The best achievable spatial resolution of conventional whole-body PET scanners is 4 to 5 mm measured using point sources, but in clinical practice the actual spatial resolution of the reconstructed images is considerably less because of the restrictions in statistics of acquired data and limitations of reconstruction algorithms. The contrast resolution also decreases with decreasing lesion size. Therefore, it is not possible to accurately measure the SUV in lesions smaller than approximately 2 to 3 times the spatial resolution of PET defined by the full width at half maximum. In addition, PET images are sampled using a voxel grid, but the voxel rarely matches the actual contour of a given lesion or a tracer's biodistribution in general.[40] Most voxels invariably include different types of tissues and the signal intensity of these voxels comprises a mixture of them. Overall, for lesions smaller than the reconstructed spatial resolution (some studies suggested <2 cm in size), PVE may result in more than 50% underestimation of the true FDG concentration, and consequently partial volume correction (PVC) is of the utmost importance. **Fig. 5** shows recovery coefficients versus diameter of spheres from a phantom study of hot spheres placed on a warm background. The recovery coefficients were calculated using SUV_{max} in the spheres and background SUV_{mean}, and were used for correction of PVE. The recovery correction versus sphere diameter showed a characteristic logarithmic curve.[41] The measurements were conducted on the Allegro PET scanner (Philips Medical Systems, Best, the Netherlands).[42]

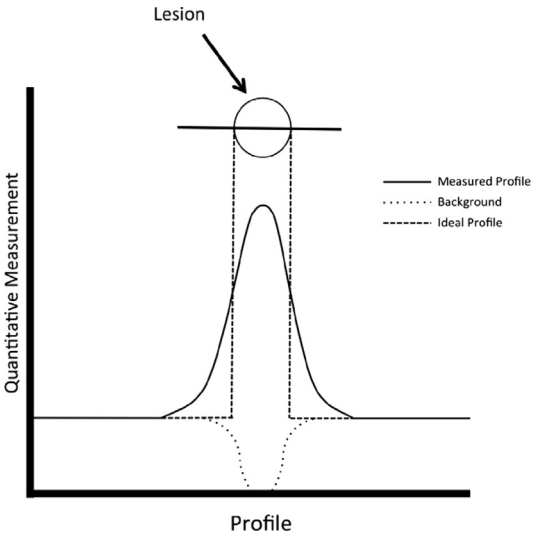

Fig. 4. The profile of a spherical lesion imaged with very high-resolution (ideal) and low-resolution PET devices. Whereas the ideal profile is noted to show a vertical increase of measured signal at the edge of the lesion, the profile of the low-resolution image is poorly defined. This phenomenon, referred to as partial volume effect, is observed in most modern imaging techniques and can be corrected by using one of the various approaches described in this article.

Several strategies have been proposed to correct for PVE,[43] but their review falls outside of the scope of this article. However, the importance of PVC cannot be overlooked in the clinical setting. Results from patients with lung cancer have shown PVC to increase the accuracy of SUV estimates from 55% to 89% in lesions less than 2 cm in size,[44] and in breast cancer, correcting SUV for PVE and blood glucose levels provided the highest diagnostic accuracy among various quantitative PET methods.[45] Similarly, a study comparing ^{110m}In-DTPA-D-Phe^1-octreotide PET images with ^{111}In-DTPA-D-Phe^1-octreotide single-photon emission CT images found great improvement in the detection of small tumors, at the same time allowing precise quantification by using PVC.[46]

OVERVIEW OF OTHER PET METRICS USED IN STATIC IMAGING

Variants of Standardized Uptake Value

Most commercial and noncommercial software packages display SUVs normalized to patient body weight (SUV_{BW}). Since the adipose tissue is less metabolically active than other tissues, it might decrease the accuracy of SUV estimation specially in obese patients. Therefore, other factors such as lean body mass (SUV_{LBM} or SUL)

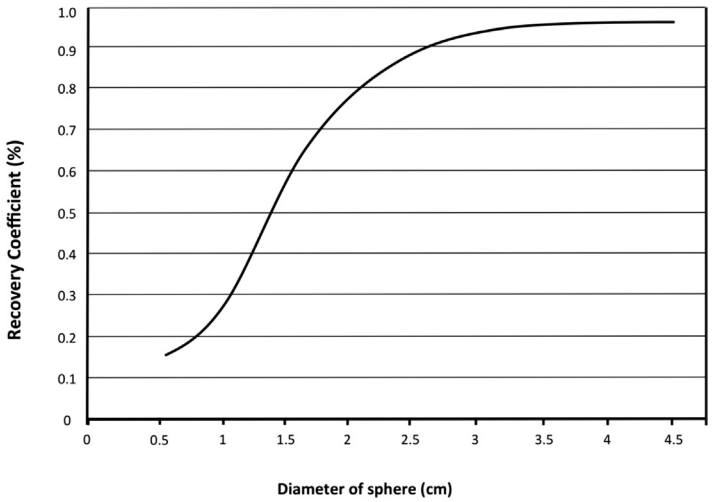

Fig. 5. Graph demonstrating the importance of the size of the lesion relative to the limited spatial resolution of PET scanners. Whereas the measured values in lesions larger than 3 cm correctly reflect the true concentration of the administered agents, such values are underestimated with smaller lesions. This phenomenon has been described as declining recovery coefficient with small lesions.

and body surface area (SUV_{BSA}) were investigated, and reported to be more accurate than the conventional method of normalization to body weight.[9,31,32] SUV_{BSA} and SUL are less prone to differences imposed by body habitus. SUL typically remains constant between patients in comparison with SUV_{BW}.[47]

Various SUV measures have been used in the literature to report the outcome of PET studies, including SUV_{max}, SUV_{mean}, SUV_{peak}, and SUV_{total}. A study by Vanderhoek and colleagues[48] has shown that quantification of individual patients is strongly affected by the SUV measure used. These investigators concluded that different SUV measures assess malignant lesions in a distinct way and that a unique threshold should be considered for each parameter for PET response classification. In PET-based treatment response assessment studies, it has been shown that SUV_{max} is strongly affected by noise. SUV_{peak} has been proposed as a more robust metric that is less vulnerable to artifacts. There are various definitions of SUV_{peak} based on the defined ROI, which can significantly affect the end result.[49]

Global Disease Burden: Assessing Global Metabolic Activity

Alavi and colleagues[50] introduced the concept of global metabolic activity in the early 1990s for assessment of patients with Alzheimer's disease in a comparison with age-matched controls. The technique consists in multiplying segmented brain volumes obtained from structural MR imaging by the mean cerebral metabolic rate of glucose, and demonstrated significant differences between the 2 groups. The concept aspires to combine volumetric and metabolic data into a unique parameter, named global disease burden or total lesion glycolysis (TLG). TLG was used as a parameter for evaluation of global metabolic response of the entire lesion in cancer.[51] It was shown that TLG is strongly correlated with other PET response parameters and is reproducible. Therefore, TLG provides complementary information to conventional SUV and its variants.

With the progress achieved in medical image segmentation, delimitation of tissues and global disease assessment has become a reality. Preliminary results obtained using commercial image analysis software have shown good reproducibility and a high level of agreement with manual measurements, indicating reasonable accuracy (**Figs. 6** and **7**).

This method has been shown to be feasible in clinical practice in malignant mesothelioma,[52] lymphoma,[53] sarcoidosis,[52] Crohn's disease,[54] radiation pneumonitis,[55] and atherosclerosis.[56–58] Using commercial software available today, FDG-avid lesions can be segmented to generate the metabolically active volume (MAV) and the partial volume corrected SUV_{mean} ($pvcSUV_{mean}$). Subsequently, the partial volume corrected metabolic volume product (pvcMVP) can be calculated as $pvcMVP_{mean} = MAV \times pvcSUV_{mean}$. Finally, a global disease activity score can be obtained as the sum of pvcMVPs in all FDG-avid lesions throughout the body. A recent article[59] reviewing current literature on metabolic tumor volume and total glycolysis in various solid tumors concluded that "both metabolic tumor volume and TLG have the potential to become valuable as prognostic biomarkers for survival outcome, clinical staging, and response to both neoadjuvant and concurrent therapies." Therefore, one can expect the development of more sophisticated and automated

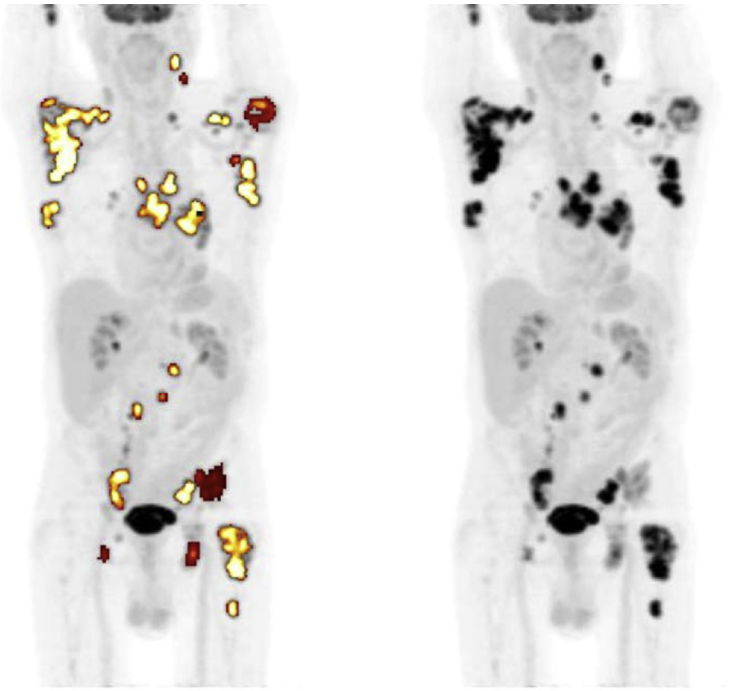

Fig. 6. FDG-PET images of a patient with non-Hodgkin lymphoma segmented using commercial software showing clearly defined FDG-avid lymph nodes throughout the body. Quantitative measures including metabolic tumor volume (MTV), SUV_{mean}, SUV_{max}, and total lesion glycolysis (TLG) can be calculated using this approach. This analysis is capable of segmenting sites of disease activity accurately while also generating corresponding quantitative parameters, as noted in the table below the image set. The values reflect MTV, SUV_{max}, SUV_{mean}, and TLG with and without partial volume correction.

MTV (cm^3)	SUVmax	SUVmean	pvcSUVmean	TLG	pvcTLG
265.9	21.1	8.4	12.86	2239.5	3541.2

software packages in the near future that can deliver these very important quantitative measures of disease activity. In essence, this may provide clinicians with a single number summing up the global disease activity of individual patients, even those presenting with multiple lesions: a simple yet robust approach to disease monitoring and assessment of treatment response.

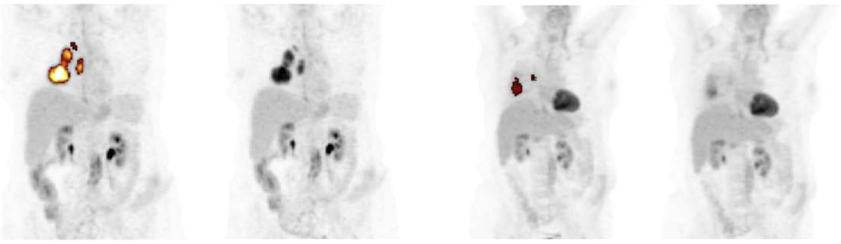

Pre-treatment Post-treatment

Timepoint	MTV (cm^3)	SUVmax	SUVmean	pvcSUVmean	TLG	pvcTLG
Pre-treatment	58.8	16.8	9.4	11.8	554.3	790.1
Post-treatment	22	7.5	4.3	6.2	94.1	135.6

Fig. 7. Images demonstrating the segmentation of metabolically active malignant lesions in a patient with lung cancer. FDG-PET scans were acquired before and after treatment. The decline in the activity of the tumor can be observed.

Texture Analysis and Radiomics

As can be concluded from the previous sections reviewing state-of-the-art developments in quantitative PET imaging, the existing quantification tools are oversimplified and subject to considerable variability. There is indeed strong evidence that relevant information can be extracted from PET images, leading to the recognition of specific markers associated with tumor molecular and genetic profiles.[60]

Texture analysis has emerged as a new approach enabling clinicians to deal appropriately with metabolic heterogeneity of malignant lesions through detailed analysis of intratumoral heterogeneity in FDG uptake.[61–63] This approach seems promising because textural features derived from PET images have proved to be of prognostic significance in solid tumors. However, further testing and assessment using large clinical databases is still required to evaluate its robustness, consistency, and limitations before the approach can be adopted in the clinic.[62]

El Naqa and colleagues[64] studied the correlation between therapy outcome and metrics derived by advanced image-processing techniques. These investigators reported a high predictive power for shape features (solidity, extent, Euler number) and texture features (energy, local homogeneity, entropy) for cancer of the cervix and head and neck, respectively. In both cases, the selected metric outperforms commonly used SUV-based descriptors. In another study, O'Sullivan and colleagues[65] developed a statistical model for sarcoma tumor delineation that identifies spatial heterogeneity as the key feature for cancer staging and prediction of patient survival. These promising results, together with the concurrent technical progress in imaging techniques and the emergence of systems biology, drove the definition of a new research domain referred to as radiomics.[66,67]

Radiomics is the science of extracting information from diagnostic images and correlating them with the biology of the tumor and the patient's clinical picture, with the aim of increasing the predictive power of medical imaging. This definition relies on the fundamental radiomics hypothesis that "tissue characteristics at the molecular level are reflected in macroscopic features of medical images and, therefore, an advanced quantitative analysis can infer genomics and proteomics patterns, possibly containing prognostic information" (www.radiomics.org). This hypothesis is supported by a few pioneering studies,[64,68,69] but more research is needed before radiomics can be adopted as a valuable and reliable tool for clinical practice.

Although high FDG uptake in PET images is associated with tumor growth and aggressiveness,[70] the biological basis for this assumption is not yet fully understood. Recent research[71,72] associates the modification of glycolysis with an agent, the pyruvate kinase isoenzyme M2 (PKM2), which is also involved in oncogenesis, thus creating a direct link between FDG uptake and tumor genetic profile. This association has been confirmed by recent research findings whereby the correlation between a set of features extracted from PET scans and the genetic profile of excised tumor specimens is tested.[73]

This discovery would legitimize the radiomics hypothesis for PET images; however, proof is still required that information can be transferred from the genetic level to clinical images.

The Critical Role of PET Image Segmentation

Image segmentation plays a pivotal role for analysis of multimodal images, and consists of techniques that group the voxels into sets of distinct classes. Segmentation has recently become a reality in clinical medicine, and is commonly used for delineation of organ and tumor volumes, generation of attenuation maps, and construction of anthropomorphic phantoms from high-resolution anatomic images.

It has been shown that discriminating the edges of malignant lesions from noisy functional images in oncology PET studies is challenging. Manual delineation is still the most widely used technique in the clinic. However, this approach is operator dependent and suffers from high interobserver and intraobserver variability, and is prone to error. Several semiautomated or fully automated techniques have been described in the literature for segmentation of lesions and other tissues from PET images.[74] Thresholding, region growing, classifiers, clustering, edge detection, Markov random fields models, artificial neutral networks, deformable models, and atlas guidance are examples of these techniques. Many of the aforementioned algorithms have been used for quantification of tumor volume and metabolic activity for either assessment of response to treatment or definition of target volumes for treatment planning.[75,76] Various strategies have also been devised to evaluate the accuracy of these segmentation techniques, including simulation and experimental phantom studies and pathology-validated clinical data sets.[77] For example, Torigian and colleagues[78] quantified pulmonary inflammation that is associated with emphysema by using FDG-PET and segmentation algorithms (**Fig. 8**). Although no correlation was noted between the severity of emphysema and the degree of inflammation in the lungs, by using CT-based segmentation a clear-cut increase in levels of FDG was shown with

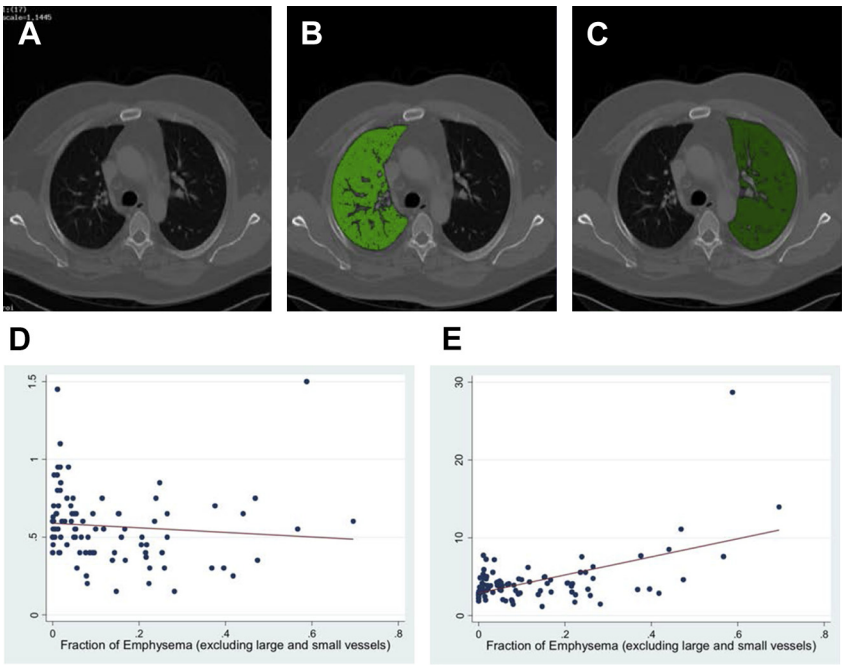

Fig. 8. Generation of graphs to measure the degree of pulmonary inflammation in patients with chronic obstructive pulmonary disease. Conventional quantitative approach by assigning regions of interest over the PET images appears flat as the degree of airway disease worsens (*D*). By contrast, by using methods that allow segmentation of air from the lung parenchyma (*A*–*C*) and applying partial volume correction, it is clear that as the disease progresses, the degree of inflammation in the remaining lung is enhanced (*E*). This result is consistent with clinical findings in these patients. ([*A*–*C*] *From* Basu S, Zaidi H, Houseni M, et al. Novel quantitative techniques for assessing regional and global function and structure based on modern imaging modalities: implications for normal variation, aging and diseased states. Semin Nucl Med 2007;37:233; with permission. [*D*, *E*] *From* Torigian DA, Dam V, Chen X, et al. In vivo quantification of pulmonary inflammation in relation to emphysema severity via partial volume corrected (18)F-FDG-PET using computer-assisted analysis of diagnostic chest CT. Hell J Nucl Med 2013;16:12–8; with permission.)

advancing disease. It should be noted, however, that none of the techniques suggested so far are characterized or understood adequately enough to enable their routine use in clinical settings without further validation.

DIFFERENTIATING BENIGN FROM MALIGNANT DISEASE USING DUAL-TIME-POINT IMAGING

Dual-time-point and delayed-time-point imaging are among the techniques used, in addition to conventional single-time-point imaging, for further characterization of inflammatory and malignant processes by enhancing the specificity of FDG-PET in certain clinical settings. Several studies have shown that the FDG uptake increases at the second time point in malignant lesions and stays at the same level or decreases in inflammatory lesions (**Fig. 9**).[79–82] Malignant cells have high levels of GLUT transporters and low levels of glucose-6-phosphatase, which leads to substantial FDG accumulation over time, whereas inflammatory lesions have high levels of glucose-6-phosphate, which results in the breakdown of FDG-6-phosphate and, therefore, clearance of FDG from the cells.[83,84]

These observations suggest that currently used PET scanning protocols, which recommend imaging at 45 to 60 minutes following the administration of FDG, may yield underestimated values for FDG uptake, which undermines the use of an arbitrarily used threshold (typically an SUV_{max} of 2.5) to differentiate between benign and malignant lesions. FDG uptake and accumulation are dynamic processes and do not stabilize until 3 to 4 hours following FDG's introduction to the circulation. In a study by Cheng and colleagues,[62] dynamic changes of FDG uptake and clearance in normal tissues were assessed in 30 patients who underwent FDG-PET imaging at 1, 2, and 3 hours after injection of FDG. FDG activity decreased with time in most organs (liver, spleen, lungs, pancreas, lymph nodes, and skeletal muscle) with an increase in activity in the myocardium and bone marrow. No changes were noted in the parotid,

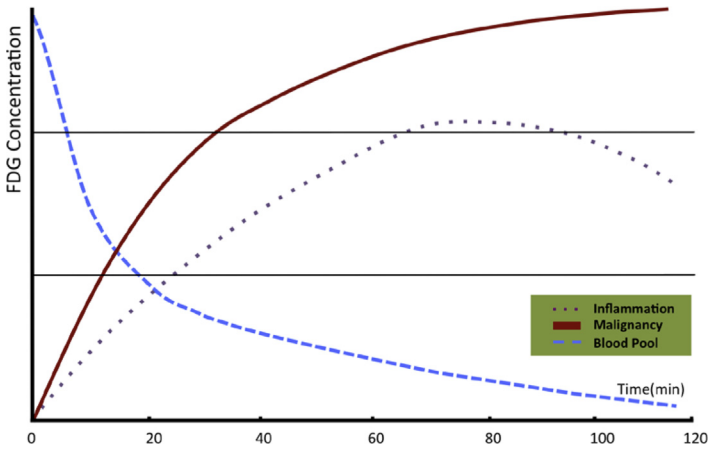

Fig. 9. Trend of FDG uptake in malignant and inflammatory lesions along with the clearance of the blood pool activity over time. Based on vast experience gained over the past 2 decades, it is now well established that malignant lesions accumulate more FDG with time. By contrast, FDG uptake either plateaus or declines in the inflammatory lesions after a certain time point.

thyroid, and prostate glands over time. An important point is that while uptake in the cancer cells increases with time and the opposite occurs in the background tissues, the enhanced contrast that follows improves the sensitivity of FDG-PET imaging (**Fig. 10**).

The hypothesis of differentiation between malignant and benign lesions using dual-time-point imaging has been confirmed by several studies. This method potentially can increase both sensitivity and specificity of the techniques in patients with suspected or proven cancer. Multiple-time-point imaging has been successfully used in several malignancies, including breast,[85,86] lung,[87] colorectal,[88] and head and neck cancer.[89] However, some studies have questioned the feasibility and applicability of dual-time-point imaging routinely and in various settings.[90,91] Further studies should be carried out with the focus on the proper applications of dual-time-point imaging in different scenarios, to clarify its role in the diagnosis and prognosis of malignant and benign diseases.

CONCLUDING REMARKS

The global emergence and deployment of hybrid PET/CT imaging enabling the combination of anatomy and morphology with functional and molecular data has brought about a paradigm shift in diagnostic imaging. Molecular imaging is now at the forefront of patient management on many levels. This powerful modality should be used not only in the initial diagnosis but also in later phases of intervention in these patients. This approach applies to surgery or other invasive procedures (interventional radiology) and in monitoring response to treatment. Using PET spares patients from futile therapeutic interventions that may not only be costly but may also subject the patients to considerable risks. The application of novel quantitative methods described in this article will enhance the performance of

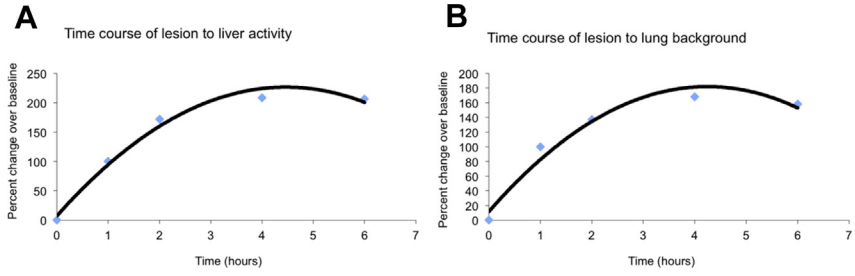

Fig. 10. Increasing contrast between malignant lesions and the surrounding background over time. The plot shown in (*A*) shows substantial increase of ratio between the lesions and the liver while graph (*B*) reveals the same between lesions and the lung. As noted in the text, the maximum contrast is not achieved until 4 hours after the administration of FDG. These graphs clearly demonstrate that imaging at 1 hour (which is the current practice in most PET imaging centers) underestimates the number of lesions and their degree of aggressiveness compared with imaging at later time points. These results seem to suggest that imaging should not be initiated until 2, and preferably 3, hours after the administration of FDG so that the benefits of this powerful imaging modality are fully realized for effective management of patients with cancer.

modern hybrid imaging modalities in variety of clinical settings, and will further improve the outcome of many serious diseases and disorders.

REFERENCES

1. Basu S, Zaidi H, Houseni M, et al. Novel quantitative techniques for assessing regional and global function and structure based on modern imaging modalities: implications for normal variation, aging and diseased states. Semin Nucl Med 2007;37:223–39.
2. Boellaard R. Optimisation and harmonisation: two sides of the same coin? Eur J Nucl Med Mol Imaging 2013;40:982–4.
3. Basu S, Kwee TC, Torigian D, et al. Suboptimal and inadequate quantification: an alarming crisis in medical applications of PET. Eur J Nucl Med Mol Imaging 2011;38:1381–2.
4. Zaidi H, Alavi A. Trends in PET quantification: opportunities and challenges. Clin Transl Imaging 2014;2:183–5.
5. Boellaard R, O'Doherty MJ, Weber WA, et al. FDG PET and PET/CT: EANM procedure guidelines for tumour PET imaging: version 1.0. Eur J Nucl Med Mol Imaging 2010;37:181–200.
6. Delbeke D, Coleman RE, Guiberteau MJ, et al. Procedure guideline for tumor imaging with ^{18}F-FDG PET/CT 1.0. J Nucl Med 2006;47:885–95.
7. Reader AJ, Zaidi H. Advances in PET image reconstruction. PET Clin 2007;2:173–90.
8. Zasadny KR, Wahl RL. Standardized uptake values of normal tissues at PET with 2-[fluorine-18]-fluoro-2-deoxy-D-glucose: variations with body weight and a method for correction. Radiology 1993;189:847–50.
9. Kim CK, Gupta NC, Chandramouli B, et al. Standardized uptake values of FDG: body surface area correction is preferable to body weight correction. J Nucl Med 1994;35:164–7.
10. Sadato N, Tsuchida T, Nakaumra S, et al. Non-invasive estimation of the net influx constant using the standardized uptake value for quantification of FDG uptake of tumours. Eur J Nucl Med 1998;25:559–64.
11. Kotasidis F, Tsoumpas C, Rahmim A. Advanced kinetic modelling strategies: towards adoption in clinical PET imaging. Clin Transl Imaging 2014;2:219–37.
12. Wang G, Qi J. Direct estimation of kinetic parametric images for dynamic PET. Theranostics 2013;3:802–15.
13. Salavati A, Saboury B, Alavi A. Comment on: "Tumor aggressiveness and patient outcome in cancer of the pancreas assessed by dynamic ^{18}F-FDG PET/CT". J Nucl Med 2014;55:350–1.
14. Rahmim A, Tang J, Zaidi H. Four-dimensional (4D) image reconstruction strategies in dynamic PET: beyond conventional independent frame reconstruction. Med Phys 2009;36:3654–70.
15. Karakatsanis NA, Lodge MA, Tahari AK, et al. Dynamic whole-body PET parametric imaging: I. Concept, acquisition protocol optimization and clinical application. Phys Med Biol 2013;58:7391–418.
16. Huang J, O'Sullivan F. An analysis of whole body tracer kinetics in dynamic PET studies with application to image-based blood input function extraction. IEEE Trans Med Imaging 2014;33:1093–108.
17. Alavi A, Reivich M, Greenberg J, et al. Mapping of functional activity in brain with ^{18}F-fluoro-deoxyglucose. Semin Nucl Med 1981;11:24–31.
18. Phelps ME, Huang SC, Hoffman EJ, et al. Tomographic measurement of local cerebral glucose metabolic rate in humans with (F-18)2-fluoro-2-deoxy-D-glucose: validation of method. Ann Neurol 1979;6:371–88.
19. Reivich M, Alavi A, Wolf A, et al. Use of 2-deoxy-D [1-^{11}C]glucose for the determination of local cerebral glucose metabolism in humans: variation within and between subjects. J Cereb Blood Flow Metab 1982;2:307–19.
20. Reivich M, Kuhl D, Wolf A, et al. The [^{18}F]fluorodeoxyglucose method for the measurement of local cerebral glucose utilization in man. Circ Res 1979;44:127–37.
21. Sokoloff L, Reivich M, Kennedy C, et al. The [^{14}C]deoxyglucose method for the measurement of local cerebral glucose utilization: theory, procedure, and normal values in the conscious and anesthetized albino rat. J Neurochem 1977;28:897–916.
22. Logan J. Graphical analysis of PET data applied to reversible and irreversible tracers. Nucl Med Biol 2000;27:661–70.
23. Zhou Y, Ye W, Brasic JR, et al. Multi-graphical analysis of dynamic PET. Neuroimage 2010;49:2947–57.
24. Schmidt KC, Lucignani G, Sokoloff L. Fluorine-18-fluorodeoxyglucose PET to determine regional cerebral glucose utilization: a re-examination. J Nucl Med 1996;37:394–9.
25. Hunter GJ, Hamberg LM, Alpert NM, et al. Simplified measurement of deoxyglucose utilization rate. J Nucl Med 1996;37:950–5.
26. Zaidi H, editor. Quantitative analysis in nuclear medicine imaging. New York: Springer; 2006.
27. Kole AC, Nieweg OE, Pruim J, et al. Standardized uptake value and quantification of metabolism for breast cancer imaging with FDG and L-[1-^{11}C]tyrosine PET. J Nucl Med 1997;38:692–6.
28. Minn H, Leskinen-Kallio S, Lindholm P, et al. [^{18}F]fluorodeoxyglucose uptake in tumors: kinetic vs. steady-state methods with reference to plasma insulin. J Comput Assist Tomogr 1993;17:115–23.
29. Keyes JW Jr. SUV: standard uptake or silly useless value? J Nucl Med 1995;36:1836–9.
30. Boellaard R. Standards for PET image acquisition and quantitative data analysis. J Nucl Med 2009;50:11S–20S.
31. Gupta NC, Frank AR, Dewan NA, et al. Solitary pulmonary nodules: detection of malignancy with PET with 2-[F-18]-fluoro-2-deoxy-D-glucose. Radiology 1992;184:441–4.

32. Kim CK, Gupta NC. Dependency of standardized uptake values of fluorine-18 fluorodeoxyglucose on body size: comparison of body surface area correction and lean body mass correction. Nucl Med Commun 1996;17:890–4.
33. Zhuang HM, Cortes-Blanco A, Pourdehnad M, et al. Do high glucose levels have differential effect on FDG uptake in inflammatory and malignant disorders? Nucl Med Commun 2001;22:1123–8.
34. Ahmadian A, Ay MR, Bidgoli JH, et al. Correction of oral contrast artifacts in CT-based attenuation correction of PET images using an automated segmentation algorithm. Eur J Nucl Med Mol Imaging 2008;35:1812–23.
35. Abdoli M, Dierckx RA, Zaidi H. Metal artifact reduction strategies for improved attenuation correction in hybrid PET/CT imaging. Med Phys 2012;39:3343–60.
36. Harnish R, Prevrhal S, Alavi A, et al. The effect of metal artefact reduction on CT-based attenuation correction for PET imaging in the vicinity of metallic hip implants: a phantom study. Ann Nucl Med 2014;28:540–50.
37. Salavati A, Borofsky S, Boon-Kent TK, et al. Application of partial volume effect correction and 4D PET in the quantification of FDG avid lung lesions. Mol Imaging Biol 2014. http://dx.doi.org/10.1007/s11307-014-0776-6, in press.
38. Bundschuh RA, Martinez-Moller A, Ziegler SI, et al. Misalignment in PET/CT: relevance for SUV and therapy management. Nuklearmedizin 2008;47:N14–5.
39. Nehmeh SA. Respiratory motion correction strategies in thoracic PET-CT imaging. PET Clin 2013;8:29–36.
40. Soret M, Bacharach SL, Buvat I. Partial-volume effect in PET tumor imaging. J Nucl Med 2007;48:932–45.
41. Srinivas SM, Dhurairaj T, Basu S, et al. A recovery coefficient method for partial volume correction of PET images. Ann Nucl Med 2009;23:341–8.
42. Surti S, Karp JS. Imaging characteristics of a 3-dimensional GSO whole-body PET camera. J Nucl Med 2004;45:1040–9.
43. Rousset O, Rahmim A, Alavi A, et al. Partial volume correction strategies in PET. PET Clin 2007;2:235–49.
44. Hickeson M, Yun M, Matthies A, et al. Use of a corrected standardized uptake value based on the lesion size on CT permits accurate characterization of lung nodules on FDG-PET. Eur J Nucl Med Mol Imaging 2002;29:1639–47.
45. Avril N, Bense S, Ziegler SI, et al. Breast imaging with fluorine-18-FDG PET: quantitative image analysis. J Nucl Med 1997;38:1186–91.
46. Lubberink M, Tolmachev V, Widstrom C, et al. 110mIn-DTPA-D-Phe1-octreotide for imaging of neuroendocrine tumors with PET. J Nucl Med 2002; 43:1391–7.
47. Wahl RL, Jacene H, Kasamon Y, et al. From RECIST to PERCIST: evolving considerations for PET response criteria in solid tumors. J Nucl Med 2009; 50(Suppl 1):122S–50S.
48. Vanderhoek M, Perlman SB, Jeraj R. Impact of different standardized uptake value measures on PET-based quantification of treatment response. J Nucl Med 2013;54:1188–94.
49. Vanderhoek M, Perlman SB, Jeraj R. Impact of the definition of peak standardized uptake value on quantification of treatment response. J Nucl Med 2012;53:4–11.
50. Alavi A, Newberg AB, Souder E, et al. Quantitative analysis of PET and MRI data in normal aging and Alzheimer's disease: atrophy weighted total brain metabolism and absolute whole brain metabolism as reliable discriminators. J Nucl Med 1993;34:1681–7.
51. Larson SM, Erdi Y, Akhurst T, et al. Tumor treatment response based on visual and quantitative changes in global tumor glycolysis using PET-FDG imaging. The visual response score and the change in total lesion glycolysis. Clin Positron Imaging 1999;2: 159–71.
52. Basu S, Saboury B, Werner T, et al. Clinical utility of FDG-PET and PET/CT in non-malignant thoracic disorders. Mol Imaging Biol 2011;13:1051–60.
53. Berkowitz A, Basu S, Srinivas S, et al. Determination of whole-body metabolic burden as a quantitative measure of disease activity in lymphoma: a novel approach with fluorodeoxyglucose-PET. Nucl Med Commun 2008;29:521–6.
54. Saboury B, Salavati A, Brothers A, et al. FDG PET/CT in Crohn's disease: correlation of quantitative FDG PET/CT parameters with clinical and endoscopic surrogate markers of disease activity. Eur J Nucl Med Mol Imaging 2014;41:605–14.
55. Abdulla S, Salavati A, Saboury B, et al. Quantitative assessment of global lung inflammation following radiation therapy using FDG PET/CT: a pilot study. Eur J Nucl Med Mol Imaging 2014;41:350–6.
56. Bural GG, Torigian DA, Chamroonrat W, et al. Quantitative assessment of the atherosclerotic burden of the aorta by combined FDG-PET and CT image analysis: a new concept. Nucl Med Biol 2006;33:1037–43.
57. Beheshti M, Saboury B, Mehta NN, et al. Detection and global quantification of cardiovascular molecular calcification by fluoro18-fluoride positron emission tomography/computed tomography–a novel concept. Hell J Nucl Med 2011;14:114–20.
58. Mehta NN, Torigian DA, Gelfand JM, et al. Quantification of atherosclerotic plaque activity and vascular inflammation using [18-F] fluorodeoxyglucose positron emission tomography/computed tomography (FDG-PET/CT). J Vis Exp 2012;(63):e3777.
59. Van de Wiele C, Kruse V, Smeets P, et al. Predictive and prognostic value of metabolic tumour volume and total lesion glycolysis in solid tumours. Eur J Nucl Med Mol Imaging 2013;40:290–301.
60. Naqa I. The role of quantitative PET in predicting cancer treatment outcomes. Clin Transl Imaging 2014;2:305–20.

61. Orlhac F, Soussan M, Maisonobe JA, et al. Tumor texture analysis in ^{18}F-FDG PET: relationships between texture parameters, histogram indices, standardized uptake values, metabolic volumes, and total lesion glycolysis. J Nucl Med 2014;55:414–22.
62. Cheng G, Alavi A, Lim E, et al. Dynamic changes of FDG uptake and clearance in normal tissues. Mol Imaging Biol 2013;15:345–52.
63. Tixier F, Hatt M, Le Rest CC, et al. Reproducibility of tumor uptake heterogeneity characterization through textural feature analysis in ^{18}F-FDG PET. J Nucl Med 2012;53:693–700.
64. El Naqa I, Grigsby PW, Apte A, et al. Exploring feature-based approaches in PET images for predicting cancer treatment outcomes. Pattern Recognit 2009;42:1162–71.
65. O'Sullivan F, Wolsztynski E, O'Sullivan J, et al. A statistical modeling approach to the analysis of spatial patterns of FDG-PET uptake in human sarcoma. IEEE Trans Med Imaging 2011;30:2059–71.
66. Aerts HJ, Velazquez ER, Leijenaar RT, et al. Decoding tumour phenotype by noninvasive imaging using a quantitative radiomics approach. Nature Comm 2014;5:4006.
67. Cook GR, Siddique M, Taylor B, et al. Radiomics in PET: principles and applications. Clin Transl Imaging 2014;2:269–76.
68. Kumar V, Gu Y, Basu S, et al. Radiomics: the process and the challenges. Magn Reson Imaging 2012;30:1234–48.
69. Lambin P, Rios-Velazquez E, Leijenaar R, et al. Radiomics: extracting more information from medical images using advanced feature analysis. Eur J Cancer 2012;48:441–6.
70. Gambhir SS. Molecular imaging of cancer with positron emission tomography. Nat Rev Cancer 2002;2:683–93.
71. Vander Heiden MG, Locasale JW, Swanson KD, et al. Evidence for an alternative glycolytic pathway in rapidly proliferating cells. Science 2010;329:1492–9.
72. Mazurek S. Pyruvate kinase type M2: a key regulator of the metabolic budget system in tumor cells. Int J Biochem Cell Biol 2011;43:969–80.
73. Nair VS, Gevaert O, Davidzon G, et al. Prognostic PET ^{18}F-FDG uptake imaging features are associated with major oncogenomic alterations in patients with resected non-small cell lung cancer. Cancer Res 2012;72:3725–34.
74. Zaidi H, El Naqa I. PET-guided delineation of radiation therapy treatment volumes: a survey of image segmentation techniques. Eur J Nucl Med Mol Imaging 2010;37:2165–87.
75. Zaidi H, Vees H, Wissmeyer M. Molecular PET/CT imaging-guided radiation therapy treatment planning. Acad Radiol 2009;16:1108–33.
76. Paulino AC, Thorstad WL, Fox T. Role of fusion in radiotherapy treatment planning. Semin Nucl Med 2003;33:238–43.
77. Kirov A, Fanchon L. Pathology-validated PET image data sets and their role in PET segmentation. Clin Transl Imaging 2014;2:253–67.
78. Torigian DA, Dam V, Chen X, et al. In vivo quantification of pulmonary inflammation in relation to emphysema severity via partial volume corrected (18) F-FDG-PET using computer-assisted analysis of diagnostic chest CT. Hell J Nucl Med 2013;16:12–8.
79. Basu S, Kung J, Houseni M, et al. Temporal profile of fluorodeoxyglucose uptake in malignant lesions and normal organs over extended time periods in patients with lung carcinoma: implications for its utilization in assessing malignant lesions. Q J Nucl Med Mol Imaging 2009;53:9–19.
80. Hamberg LM, Hunter GJ, Alpert NM, et al. The dose uptake ratio as an index of glucose metabolism: useful parameter or oversimplification? J Nucl Med 1994;35:1308–12.
81. Lodge MA, Lucas JD, Marsden PK, et al. A PET study of ^{18}FDG uptake in soft tissue masses. Eur J Nucl Med 1999;26:22–30.
82. Zhuang H, Pourdehnad M, Lambright ES, et al. Dual time point ^{18}F-FDG PET imaging for differentiating malignant from inflammatory processes. J Nucl Med 2001;42:1412–7.
83. Pauwels EK, Ribeiro MJ, Stoot JH, et al. FDG accumulation and tumor biology. Nucl Med Biol 1998;25:317–22.
84. Rosen EL, Eubank WB, Mankoff DA. FDG PET, PET/CT, and breast cancer imaging. Radiographics 2007;27(Suppl 1):S215–29.
85. Kumar R, Loving VA, Chauhan A, et al. Potential of dual-time-point imaging to improve breast cancer diagnosis with (18)F-FDG PET. J Nucl Med 2005;46:1819–24.
86. Mavi A, Urhan M, Yu JQ, et al. Dual time point ^{18}F-FDG PET imaging detects breast cancer with high sensitivity and correlates well with histologic subtypes. J Nucl Med 2006;47:1440–6.
87. Matthies A, Hickeson M, Cuchiara A, et al. Dual time point ^{18}F-FDG PET for the evaluation of pulmonary nodules. J Nucl Med 2002;43:871–5.
88. Lee JW, Kim SK, Lee SM, et al. Detection of hepatic metastases using dual-time-point FDG PET/CT scans in patients with colorectal cancer. Mol Imaging Biol 2011;13:565–72.
89. Hustinx R, Smith RJ, Benard F, et al. Dual time point fluorine-18 fluorodeoxyglucose positron emission tomography: a potential method to differentiate malignancy from inflammation and normal tissue in the head and neck. Eur J Nucl Med 1999;26:1345–8.
90. Cheng G, Torigian DA, Zhuang H, et al. When should we recommend use of dual time-point and delayed time-point imaging techniques in FDG PET? Eur J Nucl Med Mol Imaging 2013;40:779–87.
91. Houshmand S, et al. The role of dual and multiple time point imaging of FDG uptake in both normal and disease states. Clin Transl Imaging 2014;2:281–93.